

Exposure Fusion

Tom Mertens¹Jan Kautz²Frank Van Reeth¹

¹Hasselt University — EDM
transationale Universiteit Limburg
Belgium

²University College London
UK

Abstract

We propose a technique for fusing a bracketed exposure sequence into a high quality image, without converting to HDR first. Skipping the physically-based HDR assembly step simplifies the acquisition pipeline. This avoids camera response curve calibration and is computationally efficient. It also allows for including flash images in the sequence. Our technique blends multiple exposures, guided by simple quality measures like saturation and contrast. This is done in a multiresolution fashion to account for the brightness variation in the sequence. The resulting image quality is comparable to existing tone mapping operators.

1. Introduction

Digital cameras have a limited dynamic range, which is lower than one encounters in the real world. In high dynamic range scenes, a picture will often turn out to be under- or overexposed. A bracketed exposure sequence [5, 17, 26] allows for acquiring the full dynamic range, and can be turned into a single high dynamic range image. Upon display, the intensities need to be remapped to match the typically low dynamic range of the display device, through a process called tone mapping [26].

In this paper, we propose to skip the step of computing a high dynamic range image, and immediately *fuse* the multiple exposures into a high-quality, low dynamic range image, ready for display (like a tone-mapped picture). We call this process *exposure fusion*; see Fig. 1. The idea behind our approach is that we compute a perceptual quality measure for each pixel in the multi-exposure sequence, which encodes desirable qualities, like saturation and contrast. Guided by our quality measures, we select the “good” pixels from the sequence and combine them into the final result.

Exposure fusion is similar to other image fusion techniques for depth-of-field extension [19] and photomontage [1]. Burt et al. [4] have proposed the idea of fusing a



(a) Exposure bracketed sequence



(b) Fused result

Figure 1. Demonstration of exposure fusion. A multi-exposure sequence is assembled directly into a high quality image, without converting to HDR first. No camera-specific knowledge, such as the response curve, had to be accounted for. Total processing time was only 3.3 seconds (1 megapixel). Image courtesy of Jacques Joffre.

multi-exposure sequence, but in the context of general image fusion. We introduce a method that can more easily incorporate desired image qualities, in particular those that are relevant for combining different exposures.

Exposure fusion has several advantages. First of all, the acquisition pipeline is simplified, no in-between HDR image needs to be computed. Since our technique is not



(a) Input images with corresponding weight maps

(b) Fused result

Figure 2. Exposure fusion is guided by weight maps for each input image. A high weight means that a pixel should appear in the final image. These weights reflect desired image qualities, such as high contrast and saturation. Image courtesy of Jacques Joffre.

physically-based, we do not need to worry about calibration of the camera response curve, and keeping track of each photograph’s exposure time. We can even add a flash image to the sequence to enrich the result with additional detail. Our approach merely relies on simple quality measures, like saturation and contrast, which prove to be very effective. Also, results can be computed at near-interactive rates, as our technique mostly relies a pyramidal image decomposition. On the downside, we cannot extend the dynamic range of the original pictures, but instead we directly produce a well-exposed image for display purposes.

2. Related Work

High dynamic range (HDR) imaging assembles a high dynamic range image from a set of low dynamic range images that were acquired with a normal camera [5, 17]. The camera-specific response curve should be recovered in order to linearize the intensities. This calibration step can be computed from the input sequence and their exposure settings.

Most display devices have a limited dynamic range and cannot directly display HDR images. To this end, *tone mapping* compresses the dynamic range to fit the dynamic range of the display device [26]. Many different tone mapping operators have been suggested with different advantages and disadvantages. Global operators apply a spatially uniform remapping of intensity to compress the dynamic range [7, 14, 24]. Their main advantage is speed, but sometimes fail to reproduce a pleasing image. Local tone mapping operators apply a spatially varying remapping [6, 8, 10, 15, 25, 29], i.e., the mapping changes for different regions in the image. This often yields more pleasing images, even though the result may look unnatural sometimes. The operators employ very different techniques to

compress the dynamic range: from bilateral filtering [8], which decomposes the image into edge-aware low and high frequency components, to compression in the gradient domain [10]. The following two local operators are related to our method. Reinhard et al. [25] compute a multi-scale measure that is related to contrast and rescales the HDR pixel values accordingly. This is in a way similar to our measures. However, our measures are solely defined per pixel. The method by Li et al. [15] uses a pyramidal image decomposition, and attenuate the coefficients at each level to compress the dynamic range. Our method is also pyramid-based, but it works on the coefficients of the different exposures instead of those of an in-between HDR image. Other tone mappers try to mimic the human visual system, e.g., to simulate temporal adaptation [20]. Instead, we aim at creating pleasing images and try to reproduce as much detail and color as possible.

Image fusion techniques have been used for many years. For example, for depth-of-field enhancement [19, 13], multimodal imaging [4], and video enhancement [23]. We will use image fusion for creating a high quality image from bracketed exposures. In the early 90’s, Burt et al. [4] have already proposed to use image fusion in this context. However, our method is more flexible by incorporating adjustable image measures, such as contrast and saturation. Goshtasby [11] also proposed a method to blend multiple exposures, but it cannot deal well with object boundaries. A more thorough discussion of these techniques is presented in Sec. 3.3.

Grundland et al. [12] cross-dissolve between two images using a pyramid decomposition [3]. We use a similar blending strategy, but employ different quality measures.

We demonstrate that our technique can be used as a simple way to fuse flash/no-flash images. Previous techniques for this are much more elaborate [9, 2] and are specifi-

cally designed for this case, whereas our method is flexible enough to handle that case as well.

3. Exposure Fusion

Exposure fusion computes the desired image by keeping only the “best” parts in the multi-exposure image sequence. This process is guided by a set of quality measures, which we consolidate into a scalar-valued weight map (see Fig. 2). It is useful to think of the input sequence as a stack of images. The final image is then obtained by collapsing the stack using weighted blending.

As with previous HDR acquisition approaches [17, 5], we assume that the images are perfectly aligned, possibly using a registration algorithm [30].

3.1. Quality Measures

Many images in the stack contain flat, colorless regions due to under- and overexposure. Such regions should receive less weight, while interesting areas containing bright colors and details should be preserved. We will use the following measures to achieve this:

- **Contrast:** we apply a Laplacian filter to the grayscale version of each image, and take the absolute value of the filter response [16]. This yields a simple indicator C for contrast. It tends to assign a high weight to important elements such as edges and texture. A similar measure was used for multi-focus fusion for extended depth-of-field [19].
- **Saturation:** As a photograph undergoes a longer exposure, the resulting colors become desaturated and eventually clipped. Saturated colors are desirable and make the image look vivid. We include a saturation measure S , which is computed as the standard deviation within the R, G and B channel, at each pixel.
- **Well-exposedness:** Looking at just the raw intensities within a channel, reveals how well a pixel is exposed. We want to keep intensities that are not near zero (underexposed) or one (overexposed). We weight each intensity i based on how close it is to 0.5 using a Gauss curve: $\exp\left(-\frac{(i-0.5)^2}{2\sigma^2}\right)$, where σ equals 0.2 in our implementation. To account for multiple color channels, we apply the Gauss curve to each channel separately, and multiply the results, yielding the measure E .

For each pixel, we combine the information from the different measures into a scalar weight map using multiplication. We opted for a product over a linear combination, as we want to enforce all qualities defined by the measures at once (i.e. like an “AND” selection, as opposed to an “OR”

selection, resp.). Similar to weighted terms of a linear combination, we can control the influence of each measure using a power function:

$$W_{ij,k} = (C_{ij,k})^{\omega_C} \times (S_{ij,k})^{\omega_S} \times (E_{ij,k})^{\omega_E}$$

with C , S and E , being contrast, saturation, and well-exposedness, resp., and corresponding “weighting” exponents ω_C , ω_S , and ω_E . The subscript ij, k refers to pixel (i, j) in the k -th image. If an exponent ω equals 0, the corresponding measure is not taken into account. The final pixel weight $\hat{W}_{ij,k}$ will be used to guide the fusion process, discussed in the next section. See Fig. 2 for an example of weight maps.

3.2. Fusion

We will compute a weighted average along each pixel to fuse the N images, using weights computed from our quality measures. To obtain a consistent result, we normalize the values of the N weight maps such that they sum to one at each pixel (i, j) :

$$\hat{W}_{ij,k} = \left[\sum_{k'=1}^N W_{ij,k'} \right]^{-1} W_{ij,k}$$

The resulting image R can then be obtained by a weighted blending of the input images:

$$R_{ij} = \sum_{k=1}^N \hat{W}_{ij,k} I_{ij,k} \quad (1)$$

with I_k the k -th input image in the sequence. Unfortunately, just applying Eq. 1 produces an unsatisfactory result. Wherever weights vary quickly, disturbing seams will appear (Fig. 4b). This happens because the images we are combining, contain different absolute intensities due to their different exposure times. We could avoid sharp weight map transitions by smoothing the weight map with a Gaussian filter, but this results in undesirable halos around edges, and spills information across object boundaries (Fig. 4c). An edge-aware smoothing operation using the cross-bilateral filter seems like a better alternative [22, 9]. However, it is unclear how to define the control image, which would tell us where the smoothing should be stopped. Using the original grayscale image as control image does not work well, as demonstrated in Fig. 4d. Also, it is hard to find good parameters for the cross-bilateral filter (i.e., for controlling the spatial and intensity influence).

To address the seam problem, we use a technique inspired by Burt and Adelson [3]. Their original technique seamlessly blends two images, guided by an alpha mask, and works at multiple resolutions using a pyramidal image decomposition. First, the input images are decomposed into

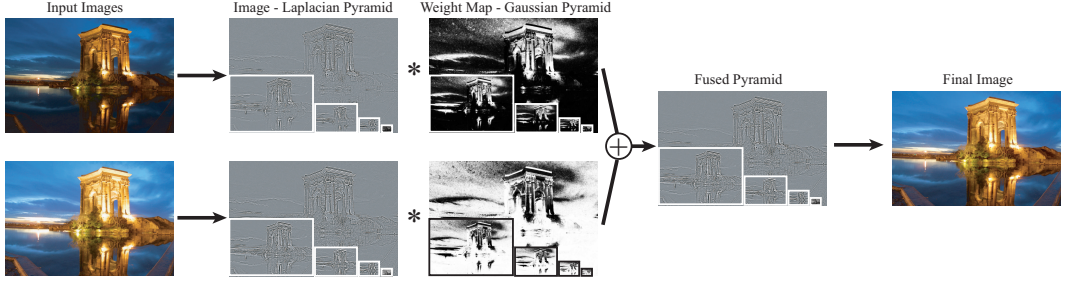


Figure 3. We fuse differently exposed images using a Laplacian decomposition of the images and a Gaussian pyramid of the weight maps, which represent measures such as contrast and saturation. Image courtesy of Jacques Joffre.

a Laplacian pyramid, which basically contains band-pass filtered versions at different scales [3]. Blending is then carried out for each level separately. We adapt the technique to our case, where we have N images and N normalized weight maps that act as alpha masks. Let the l -th level in a Laplacian pyramid decomposition of an image A be defined as $\mathbf{L}\{A\}^l$, and $\mathbf{G}\{B\}^l$ for a Gaussian pyramid of image B . Then, we blend the coefficients (pixel intensities in the different pyramid levels) in a similar fashion to Eq. 1:

$$\mathbf{L}\{R\}_{ij}^l = \sum_{k=1}^N \mathbf{G}\{\hat{W}\}_{ij,k}^l \mathbf{L}\{I\}_{ij,k}^l$$

I.e., each level l of the resulting Laplacian pyramid is computed as a weighted average of the original Laplacian decompositions for level l , with the l -th level of Gaussian pyramid of the weight map serving as the weights. Finally, the pyramid $\mathbf{L}\{R\}^l$ is collapsed to obtain R . An overview of our technique is given in Figure 3.

Multiresolution blending is quite effective at avoiding seams (Fig. 4), because it blends image features instead of intensities. Since the blending equation (1) is computed at each scale separately, sharp transitions in the weight map can only affect sharp transitions appear in the original images (e.g. edges). Conversely, flat regions in the original images will always have negligible coefficient magnitude, and are thus not affected by possibly sharp variations in the weight function, even though the absolute intensities among the inputs could be different there.

For dealing with color images, we have found that carrying out the blending each color channel separately produces good results.

3.3. Discussion

Seamless blending is an often-encountered problem in image processing and graphics. We use a multiresolution technique based on image pyramids [3], but other methods

are available as well. In particular, gradient-based blending [21] has shown to be effective, and it has been applied to image fusion as well [1, 23]. Gradient methods convert images to gradient fields first, apply the blending operation, and reconstruct the final image from the resulting gradients. However, reconstruction requires solving a partial differential equation, which can be costly for high resolution images. In addition, gradient-based fusion incurs a scale and shift ambiguity, and is prone to color shifting [23].

Tone mapping operators may also cause color shifts like oversaturation [15], and possibly reduce contrast (see Fig. 7). Our blending is robust against changes in appearance, as it can be seen as a selection process. Even though we select based on contrast and saturation, we do not directly change pixels to meet these constraints.

Our work bears similarity to early work on image fusion, where the Laplacian (or another) pyramid decomposition is used as well [19, 28, 4]. These methods work directly on the coefficients by retaining only those pyramid coefficient that are most salient. For instance, the coefficients with the largest magnitude are kept [19]:

$$\mathbf{L}\{R\}_{ij}^l = \operatorname{argmax}_{\mathbf{L}\{I\}_{ij,k}^l} |\mathbf{L}\{I\}_{ij,k}^l|$$

Burt and Kolczynski's exposure fusion technique [4] is based on the same principle. These approaches compound all details present in the sequence, but they do not necessarily produce an appealing result; see Fig. 5. Instead, we blend the pyramid coefficients based on a scalar weight map, but do not directly process individual coefficients at different levels. Measures like saturation and well-exposedness are hard to evaluate directly from pyramid coefficients. Our technique basically decouples the weighting from the actual pyramid contents, which enables us to more easily define quality measures. In fact, any measure that can be computed per-pixel, or perhaps in a very small neighborhood, is applicable.

Goshtasby's technique [11] selects the optimal exposure

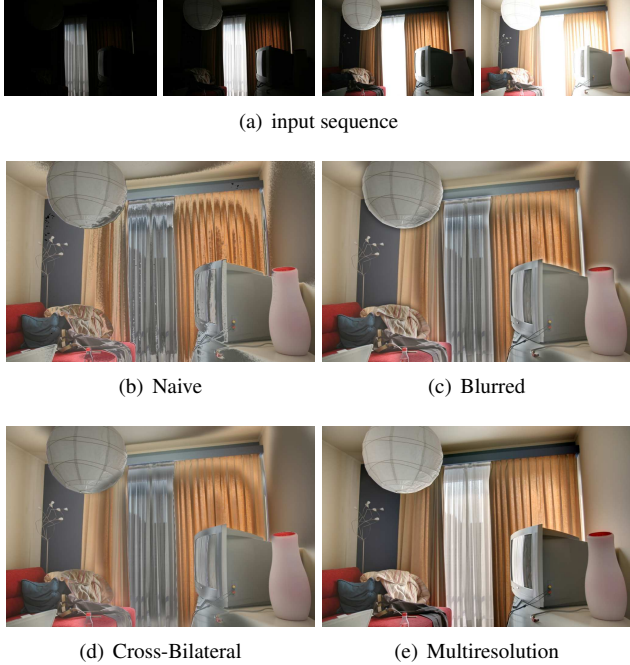


Figure 4. Weighted blending. The input sequence is shown in (a). Naive per-pixel blending (b) yields obvious seams due to sharp variations in the weight map. Blurring the weight map using a Gaussian kernel (c) removes the seams, but introduces halos around edges. Cross-bilateral filtering (d) is able to avoid some of the halos, but not all. Multiresolution blending (e) creates the desired result.

on a per-block basis, and smoothly blends between blocks. Since blocks may span across different objects, spill information across object boundaries, similar to the artifacts related to Gaussian blurring of the weight map (Fig. 4c).

4. Results

All of our examples were constructed from JPG-encoded photographs, with unknown gamma correction and camera response curve. We used equally weighted quality measures ($\omega_C = \omega_S = \omega_E = 1$) in most examples, except where mentioned otherwise.

4.1. Quality

Fig. 1 and 2 show a typical bracketed exposure shot: underexposed, normally exposed and overexposed. Every exposure contains relevant information that is not present

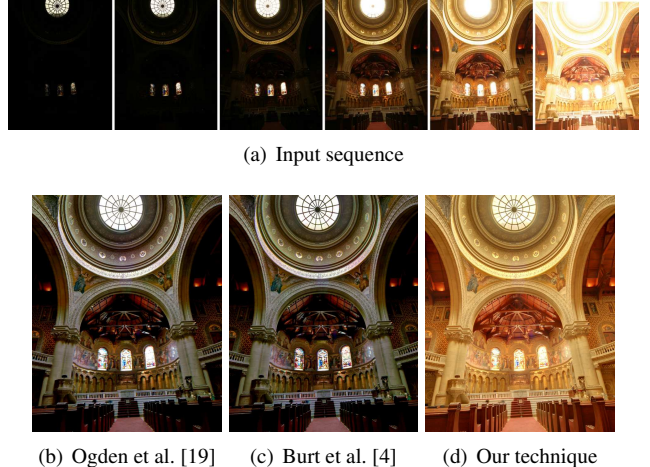


Figure 5. Comparison with other pyramid-based fusion techniques [19, 4]. These methods select the most salient Laplacian pyramid coefficients in the input sequence (a), whereas our technique does blending. The results (b,c) are too dark, and exhibit color shifts. Our technique (d) produces a more faithful result compared to the input sequence (a). Image courtesy of Jesse Levinson.

in the other exposures. Our technique is able to preserve finescale details of the buildings, and the warm appearance of the sky.

In Fig. 7 and 9, we compare our result to tone mapping. A rigorous comparison is hard, due to the operators' implementation-specific differences and parameter settings. We therefore limit ourselves to an informal comparison with a few popular tone mappers. Compared to Durand et al. [8] and Reinhard et al. [25], our method offers better contrast. Li et al.'s approach [15] produces quite similar results to ours in terms of contrast, but it also exhibits slight oversaturation. We had to tweak the saturation parameter in their implementation to correct the colors.

The multiresolution blending technique discussed in Sec. 3.2 is not without its problems. In Fig. 6, our result contains a spurious low frequency brightness change, which is not present in the original image set. It is caused by a highly varying change in brightness among the different exposures. Intuitively speaking, this artifact can be considered as a very blurred version of the seam problem, illustrated in Fig. 4b. Constructing a higher Laplacian pyramid partially solves this problem. However, the pyramid height is also limited by the size of the downsampling/upsampling filter [3].

$w \times h \times N$	init. (s)	update (s)	total (s)
$864 \times 576 \times 3$.75	.82	1.6
$1227 \times 818 \times 3$	1.5	1.6	3.2
$1728 \times 1152 \times 3$	3.0	3.2	6.2
$864 \times 576 \times 7$	1.5	1.5	3.0
$1227 \times 818 \times 7$	3.0	3.1	6.1
$1728 \times 1152 \times 7$	6.0	6.0	12.0

Table 1. Computation times for our technique. We computed results for $\frac{1}{2}$, 1 and 2 megapixel images. N is the number of images in the stack. The initialization builds the Laplacian pyramids for each input image. The update step computes the weight maps, the corresponding Gaussian pyramids, and the blending. For small image sizes (half to one megapixel), the user gets interactive interactive feedback (about one second).

4.2. Performance

Our unoptimized software implementation performs exposure fusion in a matter of seconds; see table 1. After building the Laplacian pyramids, our technique can provide near-interactive feedback (see timings of update step). This enables a user gain more control over the fusion process, as he or she can adjust the weighting of quality measures. Additional controls on the input images, such as linear and non-linear intensity remappings are also possible (like brightness adjustment or gamma curves). This can be used to give certain exposures more influence. Motivated by the work of Strengert et al. [27], we expect that our algorithm could eventually run in real-time on graphics hardware.

4.3. Including Flash-Exposures

A flash exposure can fill in a lot of detail, but tends to produce unappealing images, and it may include spurious highlights and reflections. Recent work on flash photography has introduced techniques for combining flash/no-flash image pairs [9, 22, 2]. Our technique can be used here as well, as our quality measures are also relevant in this case. Fig. 8 shows how our technique has successfully removed a highlight and filled in details, similar to Agrawal et al. [2]. However, it cannot remove flash shadows [9] or unwanted reflections [2].

4.4. Comparison of Quality Measures

Fig. 10 shows a comparison of our quality measures. Exposure fusion is performed with either contrast, saturation or well-exposedness. The desk scene in the first row



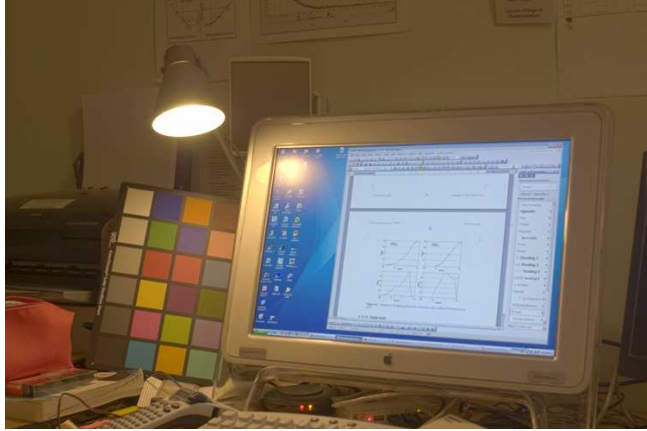
Figure 6. A spurious low-frequency change in brightness might occur due to the difference in exposure among the input images. The result (a) appears too bright toward the bottom, which seems unnatural compared to the input images. One of the input images is shown in (b) for reference.

comes out better with saturation turned on. Contrast makes the background a bit dark, and well-exposedness darkens the center of the monitor, making the result look unnatural. For the house scene on the next row, saturation and well-exposedness produce vivid colors, which is less so for contrast. Finally, the last row shows how contrast retains details, which are not present in the saturation image (e.g. in the water, and the buildings' windows). Well-exposedness yields an interesting image, but it looks less natural than the other two.

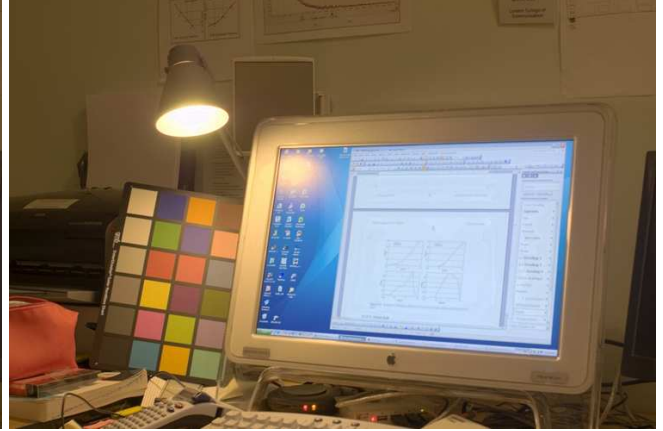
In general, we found that well-exposedness by itself produces fairly good images. However, in some cases it tends to create an unnatural appearance, because it always favors intensities around 0.5. Saturation and contrast does not have this problem. But then again, the results from those measures are not always as interesting as those produced by well-exposedness.

5. Conclusion

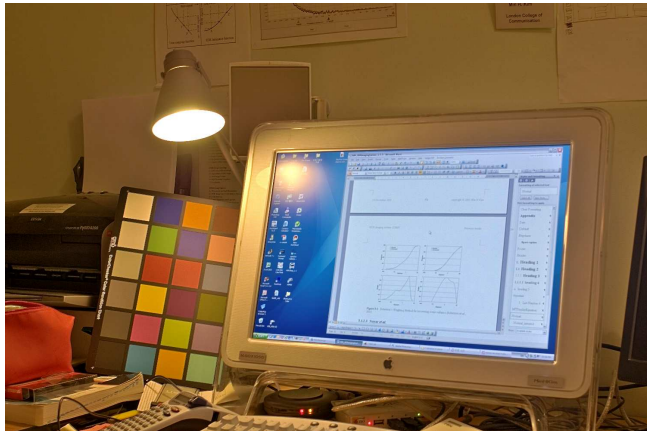
We proposed a technique for fusing a bracketed exposure sequence into a high quality image, without converting to HDR first. Skipping the physically-based HDR assembly step simplifies the acquisition pipeline. It avoids camera response curve calibration, it is computationally efficient, and allows for including flash images in the sequence.



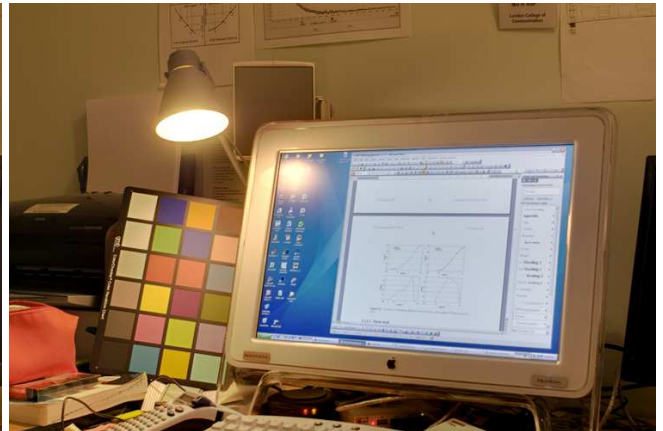
(a) Durand et al. [8]



(b) Reinhard et al. [25]



(c) Li et al. [15]



(d) Our technique

Figure 7. Comparison with several popular tone mapping techniques. Our algorithm yields image quality that is competitive with the other results. See Fig. 9 for a more detailed inspection.

Our technique blends images in a multi-exposure sequence, guided by simple quality measures like saturation and contrast. This is done in a multiresolution fashion to account for the brightness variation in the sequence. Quality is comparable to existing tone mapping operators. Our approach is controlled by only a few intuitive parameters, which can be updated at near-interactive rates in our unoptimized implementation.

We would like to investigate different pyramidal image decompositions, such as wavelets and steerable pyramids. Also, we would like to include more measures, in particular one that would detect camera noise. An optimized GPU implementation would enable the user to interactively control the fusion process, but could also be used to display a multi-exposure video stream [18] in real-time. Finally, we would like to look into the applicability of our technique to other image fusion tasks, such as depth-of-field exten-

sion [19] and multimodal imaging [4].

Acknowledgements

Thanks to Jacques Joffre, Jesse Levinson, Min H. Kim and Agrawal et al. [2] for sharing their photographs.

Part of the research at Expertise Centre for Digital Media (EDM) is funded by the European Regional Development Fund.

References

- [1] A. Agarwala, M. Dontcheva, M. Agrawala, S. M. Drucker, A. Colburn, B. Curless, D. Salesin, and M. F. Cohen. Interactive digital photomontage. *ACM Trans. Graph.*, 23(3):294–302, 2004.



Figure 8. Combining a flash/no-flash image pair using our technique. Notice how the highlight is removed, while detail and contrast has been transferred to the face. Images taken from Agrawal et al. [2].

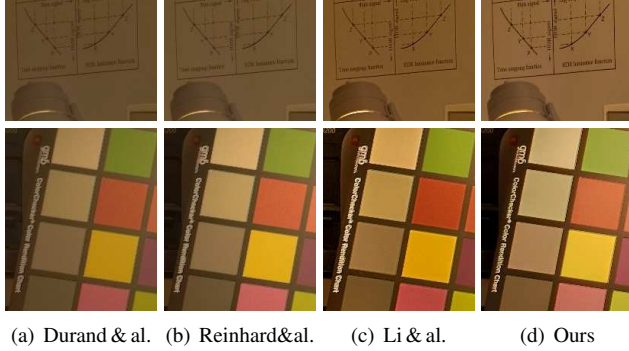


Figure 9. Comparison with several tone mapping techniques: closeups from Fig. 7. The results produced by our algorithm exhibit high contrast and good color reproduction.

- [2] A. Agrawal, R. Raskar, S. K. Nayar, and Y. Li. Removing photography artifacts using gradient projection and flash-exposure sampling. *ACM Trans. Graph.*, 24(3):828–835, 2005.
- [3] P. Burt and T. Adelson. The Laplacian Pyramid as a Compact Image Code. *IEEE Transactions on Communication*, COM-31:532–540, 1983.
- [4] P. J. Burt, K. Hanna, and R. J. Kolczynski. Enhanced image capture through fusion. In *Proceedings of the Workshop on Augmented Visual Display Research*, pages 207–224. NASA – Ames Research Center, Dec. 1993.
- [5] P. E. Debevec and J. Malik. Recovering high dynamic range radiance maps from photographs. In *SIGGRAPH ’97: Proceedings of the 24th annual conference on Computer graphics and interactive techniques*, pages 369–378, New York, NY, USA, 1997. ACM Press/Addison-Wesley Publishing Co.
- [6] J. DiCarlo and B. Wandell. Rendering high dynamic range images,. In *Proceedings of SPIE*, volume 3965, Jan. 2000.

- [7] F. Drago, K. Myszkowski, T. Annen, and N. Chiba. Adaptive logarithmic mapping for displaying high contrast scenes. *Computer Graphics Forum*, 22:419–426, 2003.
- [8] F. Durand and J. Dorsey. Fast bilateral filtering for the display of high-dynamic-range images. *ACM Trans. Graph.*, 21(3):257–266, 2002.
- [9] E. Eisemann and F. Durand. Flash photography enhancement via intrinsic relighting. In *ACM Transactions on Graphics (Proceedings of Siggraph Conference)*, volume 23. ACM Press, 2004.
- [10] R. Fattal, D. Lischinski, and M. Werman. Gradient domain high dynamic range compression. *ACM Transactions on Graphics*, 21(3):249–256, July 2002.
- [11] A. Goshtasby. Fusion of multi-exposure images. *Image and Vision Computing*, 23:611–618, 2005.
- [12] M. Grundland, R. Vohra, G. P. Williams, and N. A. Dodgson. Cross dissolve without cross fade: Preserving contrast, color and salience in image compositing. *Computer Graphics Forum*, 25(3):577–586, Sept. 2006.
- [13] P. Haeberli. A multifocus method for controlling depth of field. <http://www.graficaobscura.com/depth/index.html>, 1994.
- [14] G. W. Larson, H. E. Rushmeier, and C. D. Piatko. A visibility matching tone reproduction operator for high dynamic range scenes. *IEEE Trans. Vis. Comput. Graph.*, 3(4):291–306, 1997.
- [15] Y. Li, L. Sharan, and E. H. Adelson. Compressing and companding high dynamic range images with subband architectures. *ACM Transactions on Graphics*, 24(3):836–844, Aug. 2005.
- [16] J. Malik and P. Perona. Preattentive texture discrimination with early vision mechanism. *Journal of the Optical Society of America*, 7(5):923–932, May 1990.
- [17] S. Mann and R. Picard. Being ‘undigital’ with digital cameras: Extending dynamic range by combining differently exposed pictures. In *Proceedings of IS&T 46th annual conference.*, pages 422–428, May 1995.
- [18] M. McGuire, W. Matusik, B. Chen, J. F. Hughes, H. Pfister, and S. Nayar. Optical splitting trees for high-precision

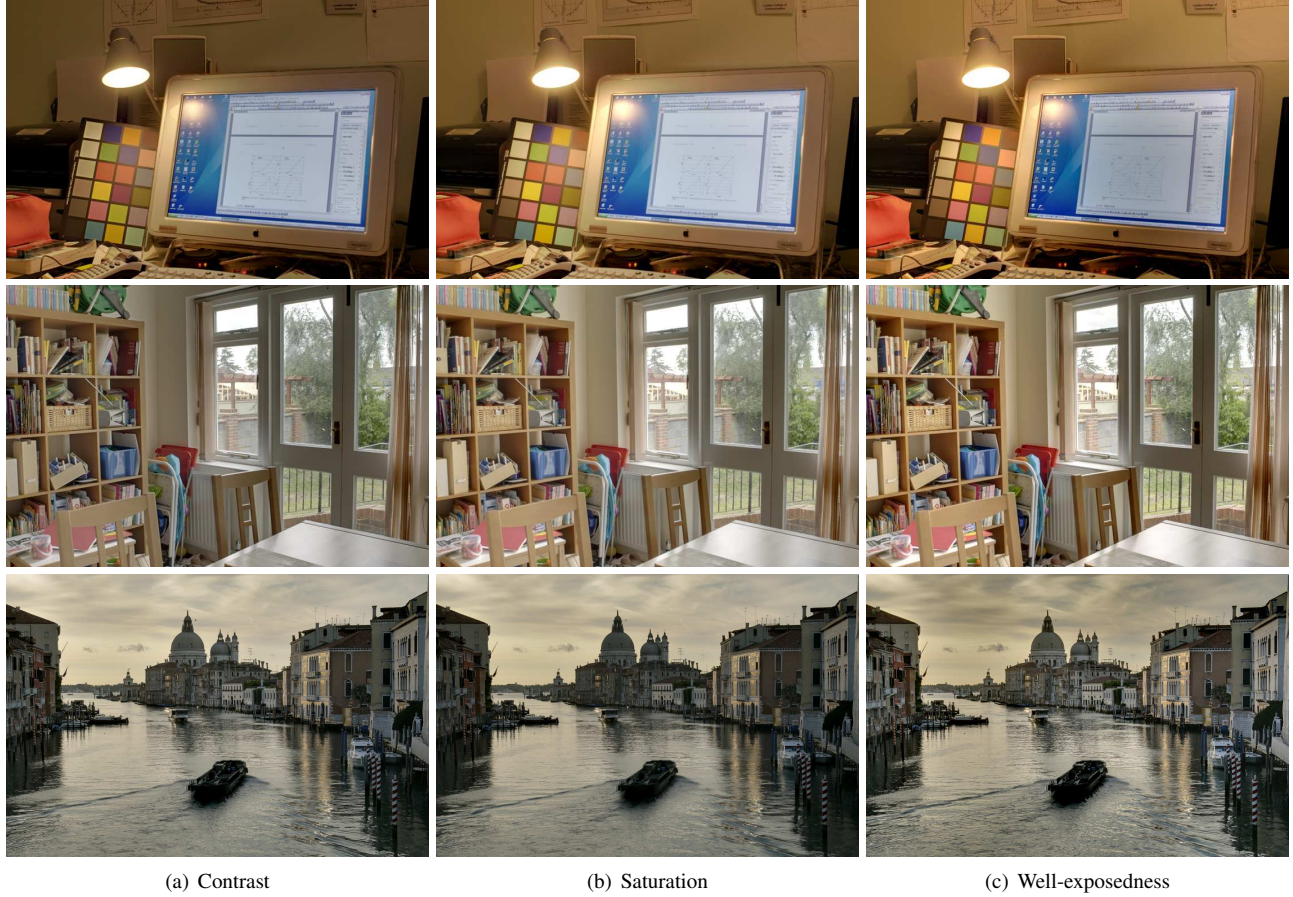


Figure 10. Comparison of our quality measures. Exposure fusion is performed with each measure turned on separately. See Sec. 4.4 for a discussion. Bottom images courtesy of Jacques Joffre.

monocular imaging. *Computer Graphics and Applications*, March 2007.

- [19] J. M. Ogden, E. H. Adelson, J. R. Bergen, and P. J. Burt. Pyramid-based computer graphics. *RCA Engineer*, 30(5), 1985.
- [20] S. N. Pattanaik, J. E. Tumblin, H. Yee, and D. P. Greenberg. Time-Dependent visual adaptation for realistic Real-Time image display. In *Proceedings of SIGGRAPH 2000, Computer Graphics Proceedings, Annual Conference Series*, pages 47–54, July 2000.
- [21] P. Pérez, M. Gangnet, and A. Blake. Poisson image editing. In *SIGGRAPH '03: ACM SIGGRAPH 2003 Papers*, pages 313–318, New York, NY, USA, 2003. ACM Press.
- [22] G. Petschnigg, R. Szeliski, M. Agrawala, M. F. Cohen, H. Hoppe, and K. Toyama. Digital photography with flash and no-flash image pairs. *ACM Trans. Graph*, 23(3):664–672, 2004.
- [23] R. Raskar, A. Ilie, and J. Yu. Image fusion for context enhancement and video surrealism. In *Proceedings of the 3rd Symposium on Non-Photorealistic Animation and Rendering*, pages 85–152, 2004.

- [24] E. Reinhard and K. Devlin. Dynamic range reduction inspired by photoreceptor physiology. *IEEE Trans. Vis. Comput. Graph*, 11(1):13–24, 2005.
- [25] E. Reinhard, M. Stark, P. Shirley, and J. Ferwerda. Photographic tone reproduction for digital images. *ACM Transactions on Graphics*, 21(3):267–276, July 2002.
- [26] E. Reinhard, G. Ward, S. Pattanaik, and P. Debevec. *High Dynamic Range Imaging: Acquisition, Display and Image-Based Lighting*. Morgan Kaufmann Publishers, Dec. 2005.
- [27] M. Strengert, M. Kraus, and T. Ertl. Pyramid Methods in GPU-Based Image Processing. In *Workshop on Vision, Modelling, and Visualization VMV '06*, pages 169–176, 2006.
- [28] A. Toet. Hierarchical image fusion. *Mach. Vision Appl.*, 3(1):1–11, 1990.
- [29] J. Tumblin and H. E. Rushmeier. Tone reproduction for realistic images. *IEEE Computer Graphics and Applications*, 13(6):42–48, Nov. 1993.
- [30] G. Ward. Fast, robust image registration for compositing high dynamic range photographs from hand-held exposures. *Journal of Graphics Tools: JGT*, 8(2):17–30, 2003.